Susceptibility of shock-transitional-boundary-layer interaction to shock oscillations in hypersonic flow

CERMINARA, Adriano, LEVIN, Deborah A. and THEOFILIS, Vassilis

Citation:

Copyright and re-use policy

Susceptibility of shock-transitional-boundary-layer interaction to shock oscillations in hypersonic flow

Adriano Cerminara[*1], Deborah Levin[†2], and Vassilis Theofilis[‡3]

[1]*Department of Engineering and Mathematics, Sheffield Hallam University, Sheffield, S1 1WB, UK*
[2]*University of Illinois at Urbana-Champaign, 104 S. Wright St. Urbana, IL 61801-2935, US*
[3]*Department of Aerospace Engineering, Technion - Israel Institute of Technology, Haifa 32000, 9 Israel*

The present study shows results from Direct Numerical Simulations (DNS) of a shock-transitional-boundary-layer interaction with imposed shock oscillations in a Mach 5 flow. The shock oscillation frequency matches the frequency predicted by a previous Direct Simulation Monte Carlo (DSMC) study for the inner thermal nonequilibrium of the shock and the resulting induced shock oscillations, for the same Mach number. The transition process is induced in the upstream region by imposed disturbance waves at the wall representative of the most unstable modes, as predicted by a Linear Stability Theory (LST) study. An oblique shock corresponding to a 8-deg wedge angle is generated at the top boundary, which impinges on the boundary layer within the region of nonlinear breakdown. Simulations have been carried out both with and without oscillations imposed on the oblique shock, and for different amplitudes of the shock oscillations. It is found that the shock-boundary-layer interaction (SBLI) produces an acceleration of the transition process to a turbulent state downstream of the impingement point, and that the shock oscillations produce a quasi-2D wave-pattern mode modulation of the downstream turbulent boundary layer, which represents the footprint of the post-shock waves generated by the shock oscillations. Increasing amplitudes of the shock oscillations show a progressively enhanced modulation of the turbulent boundary layer, with higher amplitude wall pressure fluctuations. These, in turn, have a relevant effect on the time-averaged wall pressure profiles, with an increasing mean wall pressure in the downstream turbulent boundary layer at increasing shock oscillation amplitudes. The wall pressure fluctuation amplitudes are found to scale linearly with the shock oscillation amplitudes in the higher amplitude range, however at lower amplitudes a higher sensitivity of the wall response to a change in amplitude of the shock oscillations is observed, suggesting that the correlated effects on the flow features may be relevant also for relatively small amplitudes of the shock oscillations.

I.   Introduction

Transition to turbulence plays a crucial role on the heat-transfer rates on the surface of hypersonic vehicles, which makes it necessary to understand the physical mechanism responsible for transition, in order to allow accurate prediction of the transition location. The shock-boundary-layer-interaction (SBLI) phenomenon is among the most relevant mechanisms that produce a dramatic increase of the aerodynamic heating, in combination with highly unsteady flow, as well as other important consequences terms of vehicle stability and control. The size of the separation bubble is highly dependent on the shock intensity and on the boundary-layer state.[1,2]   The separation length was found linearly dependent on the shock intensity in the experiments of Hakkinen et al.[3]   and the numerical simulations of Katzer.[4]   Lusher and Sandham[5] numerically studied the effects of flow confinement on a laminar SBLI, and found that both duct aspect ratio and the expansion fan at the trailing edge of the shock generator highly affect the interaction. Babinsky and

---

*Senior Lecturer in Aerospace Engineering, AIAA Member
†Professor of Aerospace Engineering
‡Professor of Aerospace Engineering

American Institute of Aeronautics and Astronautics

Harvey[6] found that the separation in SBLI is highly dependent on the state of the upstream boundary layer. While the flow characteristics of laminar SBLI have been studied extensively and are well established in the literature, the case of SBLI in transitional and turbulent boundary layers have not been fully understood yet. A numerical study of Sivasubramanian and Fasel[7] showed that upstream disturbances are strongly amplified by the laminar separation bubble, with transition to turbulence occurring at larger shock intensities. In the work of Sansica et al.,[8] the introduction of unstable oblique modes in a laminar SBLI led to transition to turbulence downstream of the reattachement point. The DNS study of Dwivedi et al.[9] at Mach 5.92 in laminar flow found a strong disturbance growth downstream of the reattachment point, in combination with unsteadiness and flow three-dimensionalisation at sufficiently high intensities of the oblique shock.

Boundary-layer receptivity concerns the study of how the boundary layer internalizes the impinging disturbances from the upstream flow, in the form of internal instability modes. In this context, the body leading edge is a highly-receptive zone, due to the non-parallel effects and the related short-scale streamwise variations of the mean flow, which, in turn, cause a wavelength-conversion process from the scale of the external forcing to that of the induced boundary-layer disturbances.[11] At hypersonic Mach numbers, however, it is well known that the small differences in phase speed between forcing waves and boundary-layer dominant modes lead to a direct excitation of these modes via a resonance mechanism at the leading edge,[12–15] without the need of a wavelength-conversion mechanism. Several numerical studies on the role of different types of freestream disturbances, particularly fast and slow acoustic waves, in the above-mentioned resonance mechanism have been carried out,[14, 19–25] which highlighted the complex wave interaction features of the leading-edge receptivity, the synchronisation with the external forcing, downstream modulation and evolution of different induced boundary-layer modes, whose type and relative significance in the transition process depend on the types and characteristics of the external impinging disturbances. However, another receptive region of the flow is represented by the shock, whose susceptibility to external as well as wall-reflected waves and to inner molecular collisions is a source of additional wave modes that propagate within the shock layer and impinge onto the boundary layer, thus modulating the whole boundary-layer receptivity process. The role of the shock as an active source of instability modes within the boundary layer has never been properly addressed, and deserves careful attention in the study of the physical mechanism of transition, as different transition scenarios can occur dependent on the characteristics disturbances radiated in the post-shock region from an oscillating shock.

Recent DSMC studies[26–28] have demonstrated the correlation between the shock bimodality and the formation of low-frequency oscillations. The bimodality behaviour is associated with the molecular nonequilibrium state inside the shock, which causes a bimodal shape of the probability distribution function (PDF) associated with two streams of molecular energies. Within the shock, the PDF peaks at two different energy values, corresponding to collisions between molecules upstream and downstream of the shock. These in turn will cause waves that are transmitted from the shock into the downstream (post-shock) flow field. This type of additional forcing due to kinetic fluctuations of the shock belongs to the category of "stochastic forcing", emphasised by Fedorov and Tumin[29] as responsible for the generation of unstable boundary-layer modes which undergo a significant amplification toward the nonlinear region and can lead to transition to turbulence. This behaviour was observed in DSMC studies of Tumuklu et al.[30] for the unsteady flow over a double cone.[30] Sawant et al.[27] developed an analytical model based on non-central chi-squared (NCCS) distributions to reproduce the bimodal PDF of the particle energy inside a normal shock. The analytical model was found to agree well with the actual distribution obtained from DSMC simulations. Moreover, the analytical PDF have been used to correlate the shape of the PDF to the DSMC-derived low fluctuation frequencies, in a Mach number range from 3 to 10, and in a temperature range from 89 K to 1420 K, showing a linear proportionality of the DSMC-derived low frequencies of the oscillations with the location of the PDF peak in energy space.

Contextually, in the DNS of Cerminara and Sandham[31] for the flow over a swept wedge a previously unseen transition mechanism has been found, which is associated with the generation at the leading edge and downstream growth of a high-spanwise wavenumber mode, whose source has been found correlated with a shock-wall wave reflection mechanism. This demonstrates that oscillations radiated from the shock can induce early transition in hypersonic flow. Moreover, in the study of Klothakis et al.,[32] induced shock oscillations in DSMC simulations have been found synchronized with boundary layer disturbances analysed through linear stability analysis (LST). The recent work of Cerminara, Levin and Theofilis[39] showed how shock oscillations at the DSMC-predicted oscillation frequencies cause generation of post-shock waves and

consequent formation of additional boundary-layer modes, including high-frequency modes, in a range of Mach numbers.

The present study aims at exploring the effect of shock oscillation amplitudes in a shock-transitional-boundary-layer-interaction case, within the concept of the shock receptivity, in order to investigate the response characteristics and susceptibility of the downstream turbulent boundary layer and relevant mean flow quantities to an oscillating incident shock.

II.   Numerical method

II.A.   Governing equations

We consider numerical solutions of the three-dimensional Navier-Stokes equations for compressible flows, written in conservation form, under the assumption of perfect gas. The set of non-dimensional conservation equations in Cartesian coordinates can be written as

$$\frac{\partial \mathbf{Q}}{\partial t} + \frac{\partial (\mathbf{F}_j)}{\partial x_j} = 0 \; ,$$

In the equation above, $\mathbf{Q}$ is the vector of the conservative variables, while $\mathbf{F}_j$ is the vector of the fluxes in Cartesian coordinates. The components of the vectors of the system in conservative form are

$$\mathbf{Q} = \begin{bmatrix} \rho \\ \rho u \\ \rho v \\ \rho w \\ \rho E \end{bmatrix} ,$$

$$\mathbf{F}_j = \begin{bmatrix} \rho u_j \\ \rho u u_j + \delta_{1j} p - \frac{1}{Re} \tau_{1j} \\ \rho v u_j + \delta_{2j} p - \frac{1}{Re} \tau_{2j} \\ \rho w u_j + \delta_{3j} p - \frac{1}{Re} \tau_{3j} \\ \rho \left(E + \frac{p}{\rho} \right) u_j - \frac{1}{Re} \left(u \tau_{1j} + v \tau_{2j} + w \tau_{3j} + \frac{\mu}{(\gamma - 1) Pr M^2} \frac{\partial T}{\partial x_j} \right) \end{bmatrix}$$

The terms ρ, ρu, ρv, ρw and ρE are the conservative variables of the system of equations, where ρ is the density, u, v and w are the velocity components respectively in the x, y and z directions, and E is the total energy per unit mass. In the flux vectors, the terms p, T, τ_{ij}, and μ are respectively the pressure, the temperature, the components of the viscous stress tensor, and the dynamic viscosity of the flow. The non-dimensional quantities are obtained through normalisation of the dimensional variables with their freestream reference values: the velocity components are normalised with the freestream main velocity (U_∞^*), the density is normalised with the freestream density (ρ_∞^*), the viscosity is normalised with the freestream dynamic viscosity (μ_∞^*), the temperature is normalised with the freestream temperature (T_∞^*), the total energy is normalised with the square of the freestream mean velocity (U_∞^{*2}), while the pressure and viscous stresses are normalised with the term $\rho_\infty^* U_\infty^{*2}$, related to the freestream dynamic pressure. Note that the superscript (*) is used to denote dimensional values. The boundary-layer displacement thickness at the inflow boundary (δ^*) is chosen as the characteristic length to normalise the length scales, while the time scales are normalised with respect to the fluid dynamic characteristic time (δ^*/U_∞^*), based on the velocity of the undisturbed flow and on the characteristic length. The terms Re, Pr, M, and γ are respectively the Reynolds, Prandtl and

American Institute of Aeronautics and Astronautics

Mach numbers, and the ratio of specific heats ($\gamma = c_p^*/c_v^*$), i.e. the dimensionless parameters of the flow. The Reynolds number is defined with respect to the boundary-layer displacement thickness at the inlet, as $Re = (\rho_\infty^* U_\infty^* \delta^*)/\mu_\infty^*$; the Prandtl number is set to 0.72 for air, and γ is equal to 1.4, as we are considering a perfect gas model. The dynamic viscosity is, in turn, expressed in terms of temperature by Sutherland's law

$$\mu = T^{3/2} \frac{1+C}{T+C} \ ,$$

where the constant C represents the ratio between the Sutherland's constant (set to 110.4 K) and the reference temperature (T_∞^*). The viscous stresses are defined in terms of the velocity derivatives, under the assumption of a Newtonian fluid, as

$$\tau_{ij} = \mu \left[\frac{\partial u_i}{\partial x_j} + \frac{\partial u_j}{\partial x_i} - \frac{2}{3} \delta_{ij} \frac{\partial u_k}{\partial x_k} \right] .$$

We also need a relation linking the total energy to the temperature, which in non-dimensional form can be expressed as

$$E = \frac{T}{\gamma(\gamma-1)M^2} + \frac{1}{2} \left(u^2 + v^2 + w^2 \right) \ .$$

Finally, the system of equations is closed by the equation of state for a perfect gas

$$p = \frac{1}{\gamma M^2} \rho T \ .$$

The system of equations in Cartesian coordinates is transformed into a system of equations in curvilinear coordinates (ξ, η, ζ) as

$$\frac{\partial \bar{\mathbf{Q}}}{\partial t} + \frac{\partial(\bar{\mathbf{F}}_j)}{\partial \xi_j} = 0.$$

The relations between the vectors in curvilinear and Cartesian coordinates are expressed by

$$\bar{\mathbf{Q}} = J\mathbf{Q}, \quad \bar{\mathbf{F}}_j = J\mathbf{F}_i \frac{\partial \xi_j}{\partial x_i},$$

with $J = \det \|\partial(x,y,z)/\partial(\xi,\eta,\zeta)\|$ being the jacobian of the transformation matrix.

The code used to carry out the numerical simulations is SBLI (Shock-Boundary-Layer-Interaction), developed over a number of years at the University of Southampton, consisting of a 4th-order central differencing scheme, as base scheme, in conjunction with a 2nd-order Harten-Yee TVD (Total-Variation-Diminishing) shock-capturing scheme,[33] as a filter step. A validation of the code can be found in De Tullio *et al.*[34]

III.   Computational domain and simulation settings

A rectangular-box computational domain for a flat plate is considered, with dimensions Lx = 300, Ly = 30, and Lz = 48. The mesh size in the different directions is $N_x = 1874$, $N_y = 201$, $N_z = 360$, and a grid stretching in the vertical direction towards the wall has been applied in order to accurately resolve the boundary layer. The present grid provides values of $\Delta y+ = 0.38$, $\Delta x+ = 9.06$, $\Delta z+ = 7.54$ at $x = 290$ within the fully developed turbulent region, hence guaranteeing DNS resolution in all the directions, according to the work of Coleman and Sandberg,[35] being the thresholds 1, 15 and 8 for $\Delta y+$, $\Delta x+$ and $\Delta z+$, respectively. The grid requirements also compare reasonably well with those described in the work of Yang et al.[37] for capturing rare high-intensity wall shear stress events. In particular, a grid resolution requirement dependent on the friction-based Reynolds number is presented for both $\Delta x+$ and $\Delta z+$ in the work of Yang et al.,[37] and our considered values of $\Delta x+$ and $\Delta z+$ are within the threshold values indicated in[37] for resolving 99 % of the wall shear-stress events at a calculated friction Reynolds number of $Re_\tau = 283$, based on the δ_{99}, within the downstream turbulent region.

Simulations are carried out at the freestream Mach number M = 5, temperature $T_\infty^* = 76.6$ K and Reynolds number Re = 12600, relative to the boundary-layer displacement thickness at the inlet, and for isothermal wall with wall temperature $T_w^* = 290$ K. The freestream and wall temperature conditions are the same as in the studies.[38] Periodic conditions are imposed at the side boundaries. The flow is initialised with the similarity boundary-layer solution for a Mach 5 flow at the specified wall temperature, whereas extrapolation, integral and zero-gradient outflow conditions are set at the inlet, top and outlet boundaries, respectively. Disturbance waves are imposed at the wall in the upstream region, as described in the work of Cerminara,[39] to induce the transition process.

At the top boundary a shock generator based on direct application of the Rankine-Hugoniot relations is imposed at the position $x = 31$, corresponding to an oblique shock generated by a 8-deg half-wedge angle at Mach 5. Simulations are performed for both the cases of fixed shock and oscillating shock. For the latter, a time-periodic streamwise displacement of the shock generator is imposed, at a frequency corresponding to the DSMC-predicted frequency of oscillation of the shock bimodality at Mach 5[27] ($f^* = 23$ kHz).

In the present contribution, the amplitude of the shock oscillations is varied such to investigate the associated effects on the SBLI structure and the downstream boundary layer. This is achieved through assigning different values of the maximum forward and backward displacement of the shock position on the top boundary. A periodic (sinusoidal) function is assigned to impose the shock displacement of the shock-generator, i.e. $x_s(t) = x_{s,f} + A\sin\frac{2\pi t}{T_p}$, where $x_{s,f}$ represents the streamwise position of the fixed shock (no imposed oscillations), i.e. $x_{s,f} = 31$, t is the dimensionless time and T_p is the dimensionless period of the shock oscillations. The dimensionless frequency f is imposed as a Strouhal number, i.e. $f = f^*\delta^*/U_\infty^*$, based on the reference length and the freestream velocity. In particular, four different values of the amplitude A are considered, namely $A = 0.5, 1, 1.5, 2$.

IV.   DNS results

Figure 1 shows a Schlieren image of the SBLI structure, for the case of oscillating shock at the highest amplitude ($A = 2$). The curvature of the incident shock related to the oscillations can be observed. Also, the figure shows a progressive fragmentation of the boundary layer as moving closer to the shock impingement point ($x \approx 127$) as well as a pronounced thickening indicating the formation of the separation bubble (as illustrated in the figure). Just downstream of the reattachment point, the reattachment shock propagating downstream can be observed, and the boundary layer appears to have a much larger degree of fragmentation, which is indicating transition to a turbulent state.

Figure 2 shows details of the turbulent boundary layer downstream of the reattachment point (for the temperature field on a xz-plane inside the boundary layer), evidencing a very rapid transition process from upstream to downstream of the shock impingement point. The SBLI interaction process is observed to accelerate the transition process already initiated in the upstream region by the imposed disturbance waves on the wall.[39] Figure 2 also shows evidence of a quasi-2D wave pattern developing within the downstream turbulent boundary layer. These wave fronts represent the footprint of the post-shock waves induced by the shock oscillations, which propagate downstream interacting with and producing a modulation of the turbulent boundary layer. The latter, in turn, is receptive to the post-shock wave forcing developing a wave mode synchronised with the external shock-induced waves, which evolves with an increasing amplitude in

American Institute of Aeronautics and Astronautics

the immediate downstream region.

Figure 3 shows the effect of the above-mentioned shock-oscillation-induced modulation process on the distribution of the pressure fluctuations on the wall at the different amplitudes of the shock oscillations. As can be seen, at increasing shock-oscillation amplitudes the amplitude of the wall pressure fluctuations increases as shown by the more pronounced wave fronts in the turbulent boundary layer region. The wave fronts appear as 2D wave structures with a consistent wavelength at every amplitude, which highlights a negligible effect of the shock-oscillations amplitude (measured as forward/backward linear displacement of the shock) on the wavelength, hence the wavenumber, of the induced waves.

Figures 4 and 5 show, respectively, streamwise profiles of the spanwise-averaged wall pressure fluctuations and of the time-avergaed and spanwise-averaged wall pressure. A progressive increase of the disturbance amplitude with the distance in the downstream region can be observed, indicating a growth in the streamwise direction of the wave mode induced into the boundary layer from the shock oscillations. The amplitude is also observed to increase at larger corresponding amplitudes of the shock oscillations, consistent with the results from figure 3. Moreover, the shock-induced disturbances within the turbulent boundary layer are shown to provide a significant effect on the mean wall pressure depicted in figure 5. As can be seen, while the peak of the wall pressure due to the SBLI structure is approximately the same at each amplitude of the shock oscillations, the wall pressure profile downstream of the reattachment point shows a pronounced dependence on the shock-oscillation amplitudes. Specifically, higher oscillation amplitudes provide an increase of the wall pressure downstream of the reattachment point, which results in a larger mean wall pressure within the turbulent boundary layer. The mean pressure in the downstream region is increased by about the 9% at the highest amplitude compared to the case of no shock oscillations (i.e. fixed incident shock).
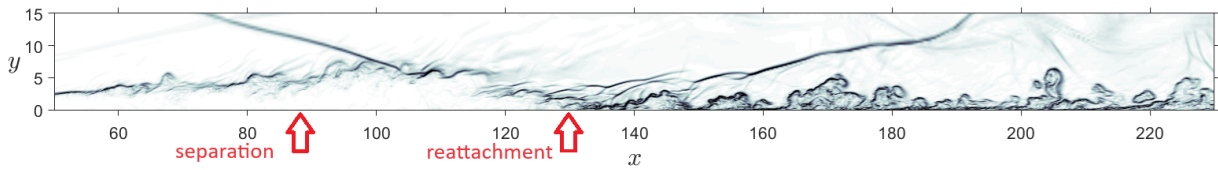

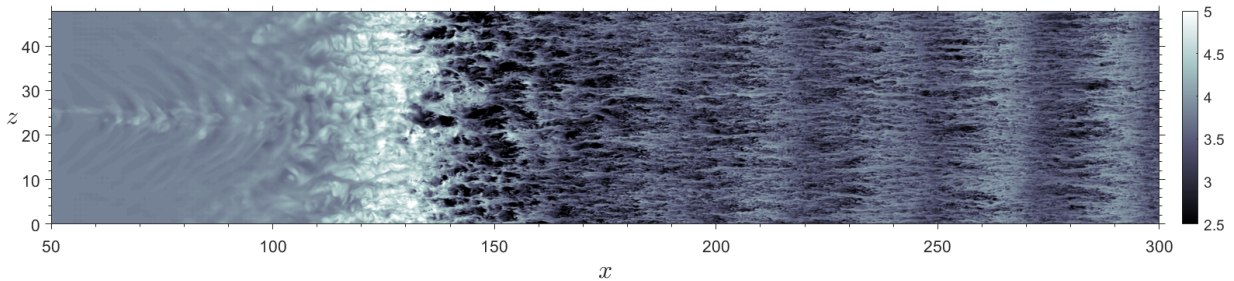Figure 1: Schlieren image in the midspan xy-plane showing the SBLI structure

Figure 2: Instantaneous temperature field in a xz-plane within the boundary layer ($y = 0.12$) at the amplitude $A = 1$
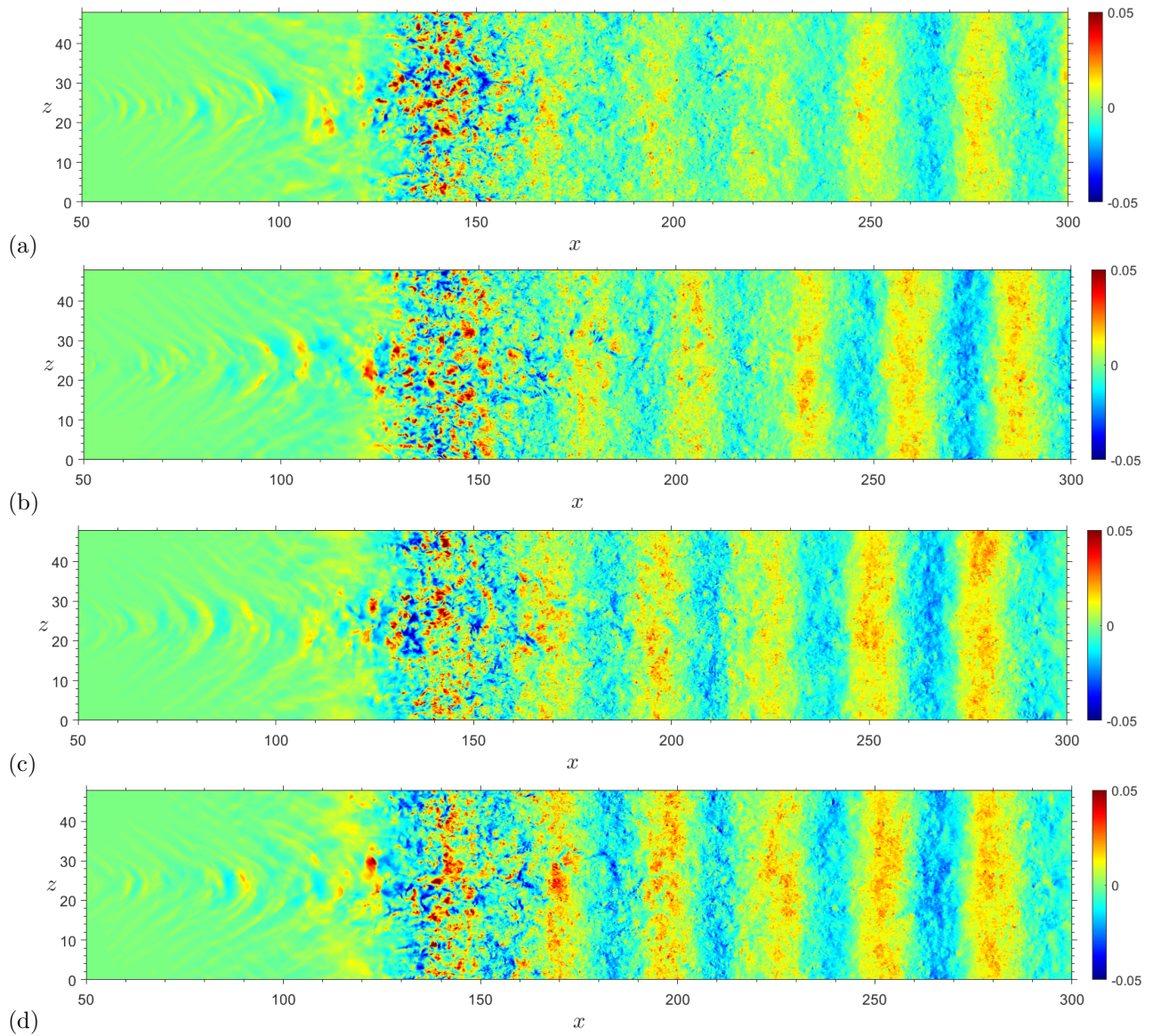
American Institute of Aeronautics and Astronautics

Figure 3: Instantaneous wall pressure fluctuation field in the surface xz-plane, respectively at $A = 0.5$ (a), $A = 1$ (b), $A = 1.5$ (c), $A = 2$ (d)

Figure 6 shows the profile of the root mean square (rms) of the wall pressure fluctuations within the turbulent boundary layer downstream of the reattachment point at increasing amplitudes of the shock oscillations. The graph shows that for the three higher amplitudes, $A = 1, 1.5, 2$, the rms scale linearly with the oscillation amplitude. In the lower amplitude range (i.e. from $A = 0.5$ to $A = 1$), however, the rms increase with a larger gradient compared to that at the higher amplitudes, thus indicating a nonlinear scaling in the low amplitude range. These results suggest that a more systematic study to accurately assess this behaviour in a wider amplitude range would be needed as object of further investigation.

Finally, figure 7 shows the streamwise profile of the time-averaged and spanwise-averaged skin-friction coefficient. To better highlight the effect of the amplitude in the downstream region, the portion upstream of the SBLI is not presented in the figure. As can be seen, the skin friction coefficient sharply increases through the SBLI region and reaches a peak at about $x = 150$. Downstream of this position, the skin friction gradually decreases within the turbulent region with the thickening of the boundary layer. A drop of the skin friction is observed in the region $x = 220 - 240$ contextually to the pressure drop shown in the same region in figure 5. The gradient associated with this decay of the skin friction appears significantly affected by the amplitude of the shock oscillations. In particular, the sharpest gradient is obtained for the case of fixed

American Institute of Aeronautics and Astronautics

shock (no oscillations), whereas the gradient becomes smoother at increasing oscillation amplitudes. This effect dependent on the amplitude of the shock oscillations, in combination with the associated effect shown on the mean wall pressure profile, can have important consequences on the vehicle aerodynamic performance, and should be further investigated in future studies.
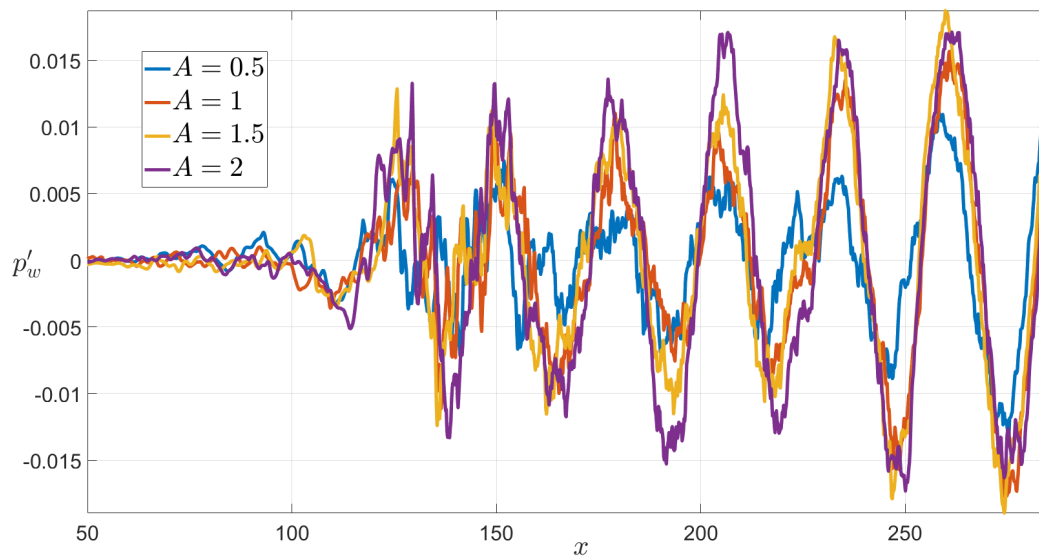

Figure 4: Streamwise distribution of instantaneous spanwise-averaged wall pressure fluctuations at different shock-oscillation amplitudes
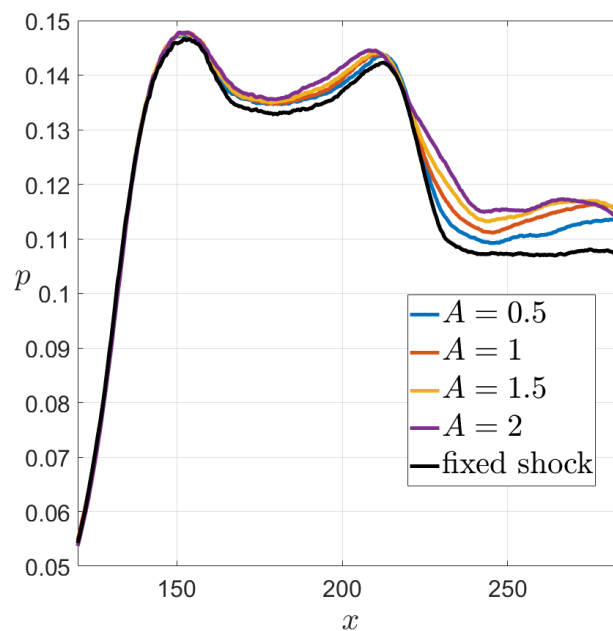

Figure 5: Streamwise distribution of time-averaged and spanwise-averaged wall pressure at different shock-oscillation amplitudes

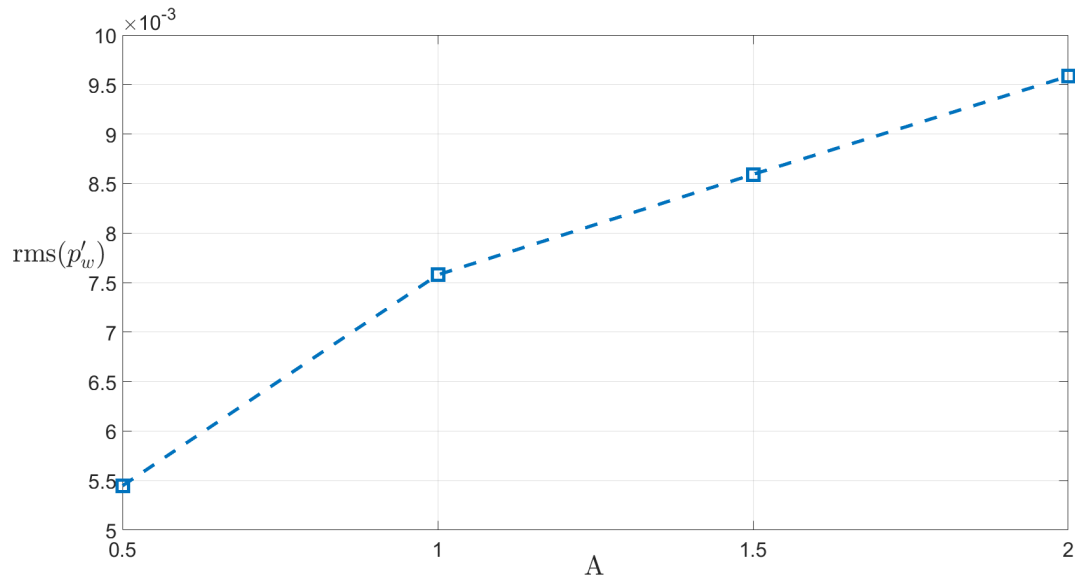American Institute of Aeronautics and Astronautics

Figure 6: RMS of the spanwise-averaged wall pressure fluctuations in the region downstream of the reattachment shock, at different amplitudes of the shock oscillations
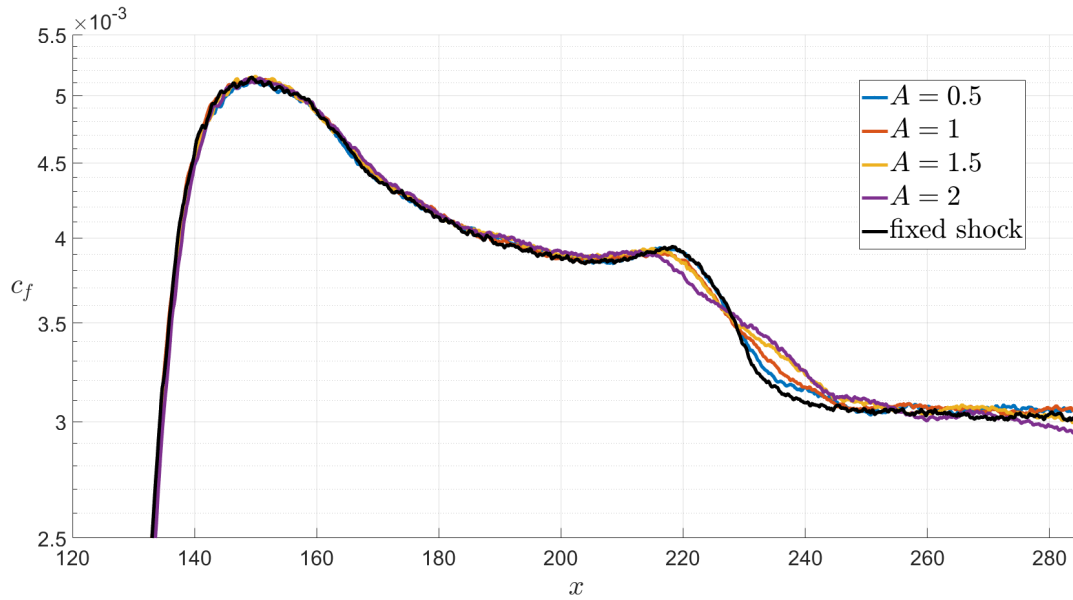

Figure 7: RMS of the spanwise-averaged wall pressure fluctuations in the region downstream of the reattachment shock, at different amplitudes of the shock oscillations

V.   Conclusion

DNS simulations have been performed for on oscillating oblique shock impinging over a transitional boundary layer in a Mach 5 flow over a flat plate, with imposed shock oscillation frequencies corresponding to those obtained in a DSMC study on the shock oscillations associated with the inner molecular nonequilibrium. Simulations have been carried out for both the cases of fixed shock and oscillating shock at different shock oscillation amplitudes, to investigate the effect of the amplitude on the SBLI and the downstream turbulent boundary-layer characteristics. It is found that the shock oscillations produce a post-shock wave field which modulates the downstream turbulent boundary layer, with evidence of pronounced quasi-2D wave fronts, spanning over the whole domain width, that keep increasing further downstream. These wave fronts observed

American Institute of Aeronautics and Astronautics

within the boundary layer represent the footprint of the post-shock waves radiated from the oscillating shock which undergo amplification downstream of the reattachment shock. It is also seen that the shock impingement on a transitional boundary layer dramatically accelerates the transition process, leading to a turbulent boundary layer with rapid fragmentation and smaller structures formed downstream of the reattachment shock. Results at different amplitudes of the shock oscillations show a more pronounced modulation effect of the turbulent boundary layer at increasing oscillation amplitudes, with higher amplitude wall pressure fluctuations. These, in turn, have a relevant effect on the time-averaged wall pressure profiles, which show a relevant increase in the downstream turbulent boundary layer at increasing shock oscillation amplitude. A 9% increase of the wall pressure in the downstream region with respect to the case of no shock oscillations is observed at the largest oscillation amplitude. The root mean square of the wall pressure fluctuations in the downstream region shows a linear scaling with the shock oscillation amplitudes in the higher amplitude range, whereas a nonlinear scaling is observed at the smaller amplitudes, where the gradient is double the gradient observed in the linear region. This suggests that at small amplitudes of the shock oscillations, an amplitude variation may cause a significant response of the boundary layer with respect to the case of fixed shock, or, in other words, the boundary layer is sensitive to the shock oscillations even for relatively small amplitudes. Profiles of the time-averaged skin friction coefficient show a progressively smoother gradient of the skin friction coefficient at larger shock oscillation amplitudes in the decrease region of the skin friction downstream of the reattachment shock, whereas the sharpest decay is observed for the case of fixed shock. The relevant effects of the shock oscillations amplitude on the mean flow quantities demonstrate the effectiveness of the shock oscillations at the DSMC-predicted frequency in modulating the turbulent boundary layer and the mean flow features downstream of the SBLI, which in turn can have a significant impact on the aerodynamic characteristics of hypersonic vehicles.

Acknowledgements

References

[1] Kiriakos, R.M., Pournadali Khamseh, A., Gianoukakis, G. and DeMauro, E.P., 2022. PIV Investigation of the Effects of Shock Generator Wedge Angle and Trailing-Edge Expansion Waves on Impinging Shock/Turbulent Boundary Layer Interactions over a Cylinder. AIAA 2022-1328 Paper.

[2] Chang, E.W.K., Chan, W.Y., McIntyre, T.J. and Veeraragavan, A., 2022. Hypersonic shock impingement studies on a flat plate: flow separation of laminar boundary layers. Journal of Fluid Mechanics, 951, p.A19.

[3] Hakkinen, R.J., Greber, I., Trilling, L. and Abarbanel, S.S., 1959. The interaction of an oblique shock wave with a laminar boundary layer (No. NASA-MEMO-2-18-59W).

[4] Katzer, E., 1989. On the lengthscales of laminar shock/boundary-layer interaction. Journal of Fluid Mechanics, 206, pp.477-496.

[5] Lusher, D.J. and Sandham, N.D., 2020. The effect of flow confinement on laminar shock-wave/boundary-layer interactions. Journal of Fluid Mechanics, 897, p.A18.

[6] Babinsky, H. and Harvey, J.K. eds., 2011. Shock wave-boundary-layer interactions (Vol. 32). Cambridge University Press.

[7] Sivasubramanian, J. and Fasel, H.F., 2015. Numerical investigation of shock-induced laminar separation bubble in a Mach 2 boundary layer. AIAA 2015-2641 Paper.

[8] Sansica, A., Sandham, N. and Hu, Z., 2013. Stability and unsteadiness in a 2D laminar shock-induced separation bubble. AIAA 2013-2982 Paper.

[9] Dwivedi, A., Nichols, J.W., Jovanovic, M.R. and Candler, G.V., 2017. Optimal spatial growth of streaks in oblique shock/boundary layer interaction. AIAA 2017-4163 Paper.

[10] Cerminara, A., Levin, D.A. and Theofilis, V., 2023. Shock receptivity: characteristics of shock oscillation modes and induced boundary-layer disturbances. AIAA 2023-0871 Paper.

[11] Saric, W., Reed, H., and Kerschen, E. *Boundary-layer receptivity to freestream disturbances*, Annual Review of Fluid Mechanics 34, 2002

[12] Fedorov, A. V., and Khokhlov, A. P. *Prehistory of Instability in a Hypersonic Boundary Layer*, Theoretical and Computational Fluid Dynamics 14 (6), 2001

[13] Fedorov, A. V. *Transition and Stability of High-Speed Boundary Layers*, Annual Review of Fluid Mechanics 43 (1), 2011

[14]Zhong, X., and Ma, Y. *Boundary-layer receptivity of Mach 7.99 flow over a blunt cone to free-stream acoustic waves*, Journal of Fluid Mechanics, 556, 2006

[15]Zhong, X., and Wang, X. *Direct Numerical Simulation on the Receptivity, Instability, and Transition of Hypersonic Boundary Layers*, Annual Review of Fluid Mechanics 44 (1), 2012

[16]Mack, L. M. *Boundary-layer linear stability theory*, Tech. Rep., California Inst. of Technology, Pasadena JPL, 1984

[17]Stetson, K. F., Thompson, E. R., Donaldson, J. C., and Siler, L. G. *Laminar boundary layer stability experiments on a cone at Mach 8. ii- blunt cone*, AIAA 22nd Aerospace Sciences Meeting, Reno, NV, 1984, https://doi.org/10.2514/6.1984-6.

[18]Fedorov, A. V., Malmuth, N. D., Rasheed, A., and Hornung, H. G. *Stabilization of hypersonic boundary layers by porous coatings*, AIAA Journal, 39 (4), pp. 605-610, 2001

[19]Ma, Y., and Zhong, X. *Receptivity of a supersonic boundary layer over a flat plate, Part 3: Effects of different types of free-stream disturbances*, Journal of Fluid Mechanics 532, 2005

[20]Balakumar, P. *Receptivity of a supersonic boundary layer to acoustic disturbances*, AIAA Journal 47 (5), 2009, pp. 1069-1078

[21]Malik, M. R., and Balakumar, P. *Acoustic receptivity of Mach 4.5 boundary layer with leading-edge bluntness*, Theoretical and Computational Fluid Dynamics, 21 (5), 2007, pp. 323-342

[22]Kara, K., Balakumar, P., and Kandil, O. A. *Receptivity of Hypersonic Boundary Layers Due to Acoustic Disturbances over Blunt Cone*, AIAA 2007-945 Paper.

[23]Egorov, I. V., Sudakov, V. G., and Fedorov, A. V. *Numerical modeling of the receptivity of a supersonic boundary layer to acoustic disturbances*, Fluid Dynamics 41 (1), 2006

[24]Cerminara, A., and Sandham, N. *Boundary-layer receptivity and breakdown in hypersonic flow over a swept blunt wedge with three-dimensional freestream acoustic disturbances, AIAA 2016-4247 Paper.*

[25]*Cerminara, A. and Sandham, N.D., 2017. Acoustic leading-edge receptivity for supersonic/hypersonic flows over a blunt wedge. AIAA Journal, 55(12), pp.4234-4244.*

[26]*Sawant, S.S., Theofilis, V. and Levin, D.A., 2022. On the synchronisation of three-dimensional shock layer and laminar separation bubble instabilities in hypersonic flow over a double wedge. Journal of Fluid Mechanics, 941.*

[27]*Sawant, S.S., Levin, D.A. and Theofilis, V., 2021. Analytical prediction of low-frequency fluctuations inside a one-dimensional shock. Theoretical and Computational Fluid Dynamics, pp.1-16.*

[28]*Sawant, S.S., Levin, D.A. and Theofilis, V., 2021. A kinetic approach to studying low-frequency molecular fluctuations in a one-dimensional shock. Physics of Fluids, 33(10), p.104106.*

[29]*Fedorov, A. and Tumin, A., 2017. Receptivity of high-speed boundary layers to kinetic fluctuations. AIAA Journal, 55(7), pp.2335-2348.*

[30]*Tumuklu, O., Theofilis, V. and Levin, D.A., 2018. On the unsteadiness of shock–laminar boundary layer interactions of hypersonic flows over a double cone. Physics of Fluids, 30(10), p.106111.*

[31]*Cerminara, A. and Sandham, N., 2020. Transition mechanisms in cross-flow-dominated hypersonic flows with free-stream acoustic noise. Journal of Fluid Mechanics, 896.*

[32]*Klothakis, A., Quintanilha, H., Sawant, S.S. et al. Linear stability analysis of hypersonic boundary layers computed by a kinetic approach: a semi-infinite flat plate at $4.5 \leq M_\infty \leq 9$. Theor. Comput. Fluid Dyn. 36, 117–139 (2022). https://doi.org/10.1007/s00162-021-00601-y*

[33]*Yee, H. C., Sandham, N. D., and Djomehri, M. J. Low-dissipative high-order shock-capturing methods using characteristic-based filters, Journal of Computational Physics 150 (1), pp. 199-238, 1999*

[34]*De Tullio, N., Paredes, P., Sandham, N. D., and Theofilis, V. Laminar-turbulent transition induced by a discrete roughness element in a supersonic boundary layer, Journal of Fluid Mechanics 735, pp. 613-646, 2013*

[35]*Coleman, G.N. and Sandberg, R.D., 2010. A primer on direct numerical simulation of turbulence-methods, procedures and guidelines. Technical Report AFM-09/01a, University of Southampton.*

[36]*Hermann, T., Ifti, H., McGilvray, M., Doherty, L. and Geraets, R., 2018. Mixing characteristics in a hypersonic flow around a transpiration cooled flat plate model. In HiSST: International Conference on High-Speed Vehicle Science Technology.*

[37]*Yang, X.I., Hong, J., Lee, M. and Huang, X.L., 2021. Grid resolution requirement for resolving rare and high intensity wall-shear stress events in direct numerical simulations. Physical Review Fluids, 6(5), p.054603.*

[38]*Cerminara, A., Deiterding, R. and Sandham, N., 2020. A mesoscopic modelling approach for direct numerical simulations of transition to turbulence in hypersonic flow with transpiration cooling. International Journal of Heat and Fluid Flow, 86, p.108732.*

[39]*Cerminara, A., 2023. Turbulence Effect on Transpiration Cooling Effectiveness Over a Flat Plate in Hypersonic Flow and Sensitivity to Injection Parameters. Flow, Turbulence and Combustion, 110(4), pp.945-968.*